Eur. Phys. J. C manuscript No.
(will be inserted by the editor)

Charge-current paper

xFitter Developers' team:

[1]Address(es) of author(s) should be given

Received: date / Accepted: date

Abstract

1 Introduction

The Deep-inelastic-scattering (DIS) experiments traditionally were an important probe of pQCD and used to precise determination of parton distribution functions (PDFs) at lepton-nucleon and nucleon-nucleon colliders. The various dedicated experiments such as HERA have been performed by colliding electron and positron with proton to investigate the nucleon structure. The broad kinematic region of charge-current (CC) and Neutral-current (NC) DIS data at HERA base on negative transverse momentum squared Q^2 and Bjorken variable x caused that these data play important role on modern determination of the parton distribution function [1–3].

In the standard model, the charm quark has an important role in the investigation of the nucleon structure [4–6]. The pQCD calculation assumed that charm charm distribution is generated perturbatively by gluon and light quark splitting functions and it's mass depended strongly on the DIS coefficient functions which is are known up to second order in the strong coupling constant in the NC process considering heavy quark mass effects[7, 8] . The heavy quark mass effects in the CC process, calculated up to $\mathcal{O}(\alpha_s^2)$ in Refs. [9–12] and recently completed in Ref. [13] which is available up to $\mathcal{O}(\alpha_s^2)$ at large Q^2 for the xF_3 structure function [14].

Although the heavy quarks specially charm quark, have an important role in many process even beyond the standard model, there are some process which is provides direct access to the strange sea quark, one of the significant part of the nucleon structure and the completed and accurate knowledge on this topic help us to the better understanding of the properties of the sea quark and also the nucleon structure in the process with a strange quark mediated by weak charge boson in association with charm jet [15, 16] and also neutrino and anti-neutrino production measured by CCFR [17], NuTev [18], CHORUS [19], CDHSW [20] and NOMAD [21] collaborations that give useful information but limited on the normalisation and shape of the $s(x)+\bar{s}(x)$. for the first time HERMES collaboration extracted the $s(x)+\bar{s}(x)$ from charged lepton DIS data and complementary to the neutrino results [22].

On the other hand the charm production mediated by electroweak gauge boson at hadron colliders provide important information on strange and charm quark distribution and complementary the DIS final state charm quark experiment [16]. Although CDF and D0 at Tevatron [23, 24] measured the charm quark cross section in association with W boson but these measurement is limited to 30% by low statistics. Some of the global QCD analyses in absence of significant experiential constraints, at some low factorisation scale, extracted the strange $s(x)$ and anti-strange $\bar{s}(x)$ given by $s(x) = \bar{s}(x) = r_s[\bar{u}+\bar{d}]/2$ [25, 26] here r_s is the fraction of the strange quark density in the proton that reported value by ATLAS at the scale $Q-0 = 1.9$ GeV^2 and $x = 0.023$ is 1.19 [27]. The LHC tried to provide a more precise measurement and CMS and ATLAS collaboration performed ... By eliminated the isoscalar between strange and anti-strange distribution, the CTEQ [16] and MSTW [28] extracted the strange and anti-strange distribution at NLO. This paper organized as follow, in the Sec. ....

[0]Preprint numbers: DESY ...
Correspondence: . . .

2 Theoretical predictions for charm CC production at LHeC

Theoretical predictions are calculated for electroweak charm CC production in ep collisions at the LHeC at centre-of-mass energy $\sqrt{s} = 1.3$ TeV, using a variety of heavy flavour schemss. The predictions are provided for unpolarised beams in the kinematic range $100 < Q^2 < 100000$ GeV^2, $0.0001 < x_{\mathrm{Bj}} < 0.25$. They are calculated as reduced cross sections at different Q^2, x_{Bj} and y points.

Experimentally, however, not charm quarks but charmed hadrons (or rather their decay products) are registered in the detectors. Therefore, extrapolation to the inclusive charm production cross section has to be carried out in a model dependent way. Furthermore, in CC charm quarks in the final state can be produced via both electroweak and QCD production processes. The former leads to an odd number of charm quarks in the final state with the W boson having the same electric charge as the sum electric charges of final state charm quarks, while the latter creates an even number of charm quarks with total electric charge equal to zero. If the electric charge of the tagged charm quark can be accessed experimentally (e.g. when reconstructing D mesons), the QCD contribution can be excluded by taking the difference of the yields in the events with odd and even numbers of charm quarks, otherwise the QCD contribution can be subtracted only in a model dependent way.

The charm CC process directly depends on the CKM matrix. Here, the CKM matrix elements V_{cd} and V_{cs} are of particular interest. The values used are $V_{cd} = 0.2252$ and $V_{cs} = 0.9734$. Three different heavy-flavour schemes are employed, all including a full treatment of charm mass effects up to NLO[1], i.e. $O(\alpha_s)$, and described here for the particular application to charged current electron-proton reactions. The standard fixed flavour number scheme (FFNS A) uses three light flavours in both PDFs and α_s evolution, while heavy flavours (here: charm) are produced exclusively in the matrix element part of the calculation. This scheme has been used e.g. for the PDF determinations and cross-section predictions of the ABM(P) group [29, 30], as well as in the FF3A variant of HERAPDF [2], and implemented in xFitter through the OPENQCDRAD package [31]. The "B" variant of the fixed-order-next-to-leading-log scheme (FONLL B) combines the NLO ($O\alpha_s$) massive matrix elements of the fixed flavour scheme with the NLO ($O\alpha_s$) massless treatment of the zero-mass variable flavour number scheme (ZM-VFNS), allowing the number of active flavours (3, 4, or 5) to vary with scale, and all-order next-to-leading log resummation of (massless) terms beyond NLO. It thus explicitly includes charm and beauty both in the PDFs and in the evolution of the strong coupling constant. Whenever terms would be double-counted in the merger of the two schemes the massless terms are eliminated in favour of retaining the massive terms. The FONLL is heavily used by the NNPDF group [Ball:2017nwa] and implemented in xFitter through the APFEL package [32]. Finally a variant of the fixed flavour number scheme known as the 'mixed' scheme or FFNS B [4] is used. In this scheme, the number of active flavours is still fixed (here: to 3) in the PDFs, relying exclusively on $O(\alpha_s)$ fully massive matrix elements for charm production, while the number of flavours is allowed to vary in the virtual corrections of the alphas evolution. Corrections to this evolution involving heavy flavour loops are thus included and resummed to all orders, as in the VFNS schemes, while no resummation is applied to other higher order corrections. This procedure will catch a large fraction of the "large logs" which might spoil the fixed-flavour scheme convergence at very high scales, and is possible since the masses of the charm and beauty quarks provide natural cutoffs for infrared and collinear divergences. This scheme was used in the HERAPDF FF3B variant [2] and in applications of the HVQDIS program [4]. In general the transition from the FFNS A to the FFNS B scheme requires a readjustement of the treatment of matrix elements involving heavy flavour loops, but in the specific case of charged current no such loops occur up to NLO (at NNLO they will), such that the same matrix elements can be used for both schemes, and here the only difference is the alphas evolution.

In summary, the schemes used are

- FFNS A with $n_f = 3$ at NLO and ABMP16 [30] or HERAPDF2.0 FF3A [2] NLO PDF set,
- FFNS B with $n_f = 3$ at NLO and ABMP16 [30] or HERAPDF2.0 FF3B [2] NLO PDF set,
- FONLL-B with $n_f = 3$ and NNPDF3.1 NLO PDF set [33].

All calculations are interfaced in xFitter and available in the scheme using the running $\overline{MS}$ charm mass, $m_c(m_c)$. The $\overline{MS}$ charm mass is set to $m_c(m_c) = 1.27$ GeV [34], and α_s is set to the value used for the corresponding PDF extraction ($\alpha_s(M_Z) = 0.1191$ for ABMP16, and $\alpha_s(M_Z) = 0.118$ for NNPDF3.1). The renormalisation and factorisation scales are chosen to be $\mu_{\mathrm{r}} = \mu_{\mathrm{f}} = Q^2$.

To estimate theoretical uncertainties, the two scales are simultaneously varied up and down by factor 2. In the case of the FONLL-B calculations, also the independent μ_r and μ_f variations are checked. Furthermore, the PDF uncertainties are propagated to the calculated theoretical predictions, while the uncertainties arising from varying the charm mass $m_c(m_c) = 1.27 \pm 0.03$ GeV are smaller than 1% and therefore neglected. In the FONLL-B scheme, as a cross check, the calculation was performed with the pole charm mass $m_c^{\mathrm{pole}} = 1.51$ GeV which is consistent with the conditions of the NNPDF3.1 extraction [33]. The obtained theoretical predictions differ from the ones calculated with $m_c(m_c) = 1.27$

[1] The $O(\alpha_s^2)$ corrections quoted earlier are not yet avaialble in the context of the xFitter setup.

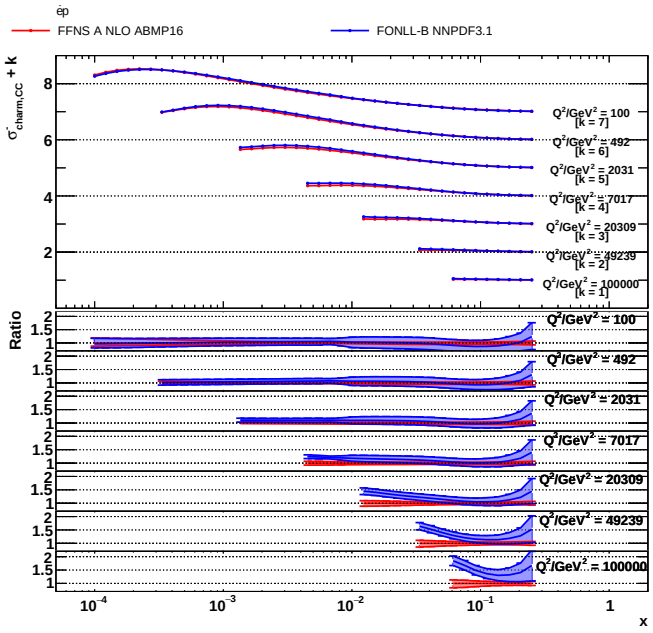

Figure 1 The theoretical predictions with their total uncertainties for charm CC production at the LHeC as a function of x_{Bj} for different values of Q^2 calculated in the FFNS A and FONLL-B schemes. The bottom panel display the theoretical predictions normalised to the nominal values of the FFNS A predictions.

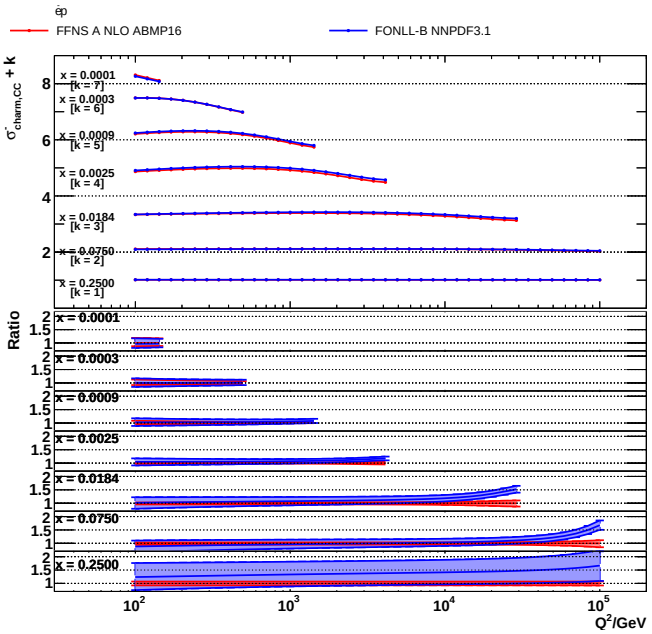

Figure 2 The theoretical predictions with their total uncertainties for charm CC production at the LHeC as a function of Q^2 for different values of x_{Bj} calculated in the FFNS A and FONLL-B schemes. The bottom panel display the theoretical predictions normalised to the nominal values of the FFNS A predictions.

GeV by less than 1%. The total theoretical uncertainties are obtained by adding in quadrature the scale and PDF uncertainties.

2.1 Comparison of theoretical predictions in the FFNS A and FONLL-B schemes

Figures 1, 2 and 3 show theoretical predictions with their total uncertainties in both schemes as a function of x_{Bj} for different values of Q^2, as a function of Q^2 for different values of x_{Bj}, and as a function of y for different values of Q^2, respectively. The FFNS A and FONLL-B agree reasonably well, within uncertainties of moderate size, in the bulk of the phase space. However, in phase space corners such as high $Q^2 \gtrsim 10000\ \mathrm{GeV}^2$ or low $y \lesssim 0.05$ the predictions in the two schemes differ by more than 50%, and these differences are not covered by the theoretical uncertainties.

In Fig. 4 the PDF and scale uncertainties of charm CC cross sections as a function of Q^2 for different values of x_{Bj} calculated in the FFNS A and FONLL-B schemes are shown. On average, in the FONLL-B scheme both the PDF and scale uncertainties exceed those in the FFNS A scheme. Furthermore, Fig. 5 shows the impact of separate scale variations in the two schemes. In the FONLL-B scheme, the variation of μ_f has a much larger impact on the predictions than the variation of μ_r, and thus it is dominant for the resulting scale uncertainties. **[Valerio, could you please dis-**

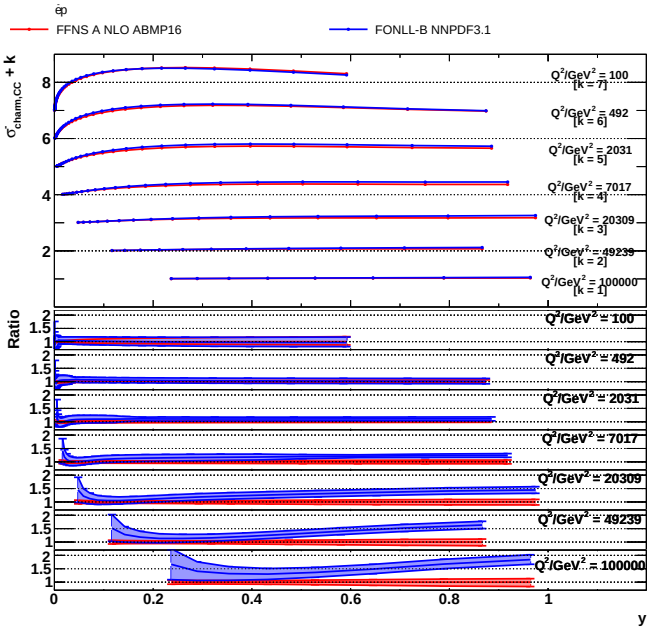

Figure 3 The theoretical predictions with their total uncertainties for charm CC production at the LHeC as a function of y for different values of Q^2 calculated in the FFNS A and FONLL-B schemes. The bottom panel display the theoretical predictions normalised to the nominal values of the FFNS A predictions.

cuss more here?] Only the simultaneous $\mu_f = \mu_r$ variation is available in the implementation of the FFNS A scheme.

To explore whether the differences between the two sets of theoretical predictions appear due to the different treatment of heavy quarks or due to different PDF sets, theoretical calculations in the FFNS A and FONLL-B schemes are repeated with PDF sets extracted from the fit to the HERA DIS data [2]. The fit settings follow the HERAPDF2.0 analysis [2]. In this study, consistent conditions of the PDF extraction eliminate possible differences between the predictions for the LHeC arising from the dissimilarities of the ABMP16 and NNPDF3.1 analysis. The obtained results are displayed in Figs. **??–??**. The differences between the FFNS A and FONLL-B schemes in these predictions are similar to the ones displayed in Figs. 1–3 and prove that these differences arise due to the different treatment of heavy quarks in the two schemes.

Furthermore, the predictions in the FFNS A and FFNS B schemes calculated using the HERAPDF2.0 FF3A and HERAPDF2.0 FF3B PDF sets are displayed in Figs. **??–??**. Because of the similarities of the two HERAPDF2.0 PDF sets, the differences between the two sets of the predictions arise mainly due to the different treatment of heavy quarks in the two schemes. Remarkably, the differences between FFNS A and FONLL-B predictions are similar to the ones between FFNS A and FFNS B, i.e. a larger part of these differences arise due to the different treatment of heavy quarks in $\alpha_s(\mu)$ running.

To explore whether the differences between the two sets of theoretical predictions appear due to the different treatment of heavy quarks or due to different PDF sets, theoretical calculations in the FFNS A and FONLL-B schemes are repeated with the HERAPDF2.0 sets extracted from the same HERA DIS data using coherent settings [2]. Furthermore, the predictions in the FFNS B scheme are produced using the HERAPDF2.0 FF3B PDF set and the FFNS A matrix elements, which are equaivalent to the FFNS B matrix elemenets at NLO for charm CC production. The obtained results are displayed in Fig. 6. The differences between the FFNS A and FONLL-B schemes in these predictions are similar to the ones displayed in Figs. 1–3 and prove that these differences arise due to the different treatment of heavy quarks in the two schemes. The FFNS B predictions are between the FFNS A and FONLL-B predictions, indicating that a large part of these differences arise due to the different treatment of heavy quarks in $\alpha_s(\mu)$ running.

Furthermore, to investigate the impact of the NNLO corrections available at $Q \gg m_c$ for the FFNS calculation, approximate NNLO predictions are obtained using the ABMP16 NNLO PDF set [29]. The results for the cross sections as a function of Q^2 for difference values of $x_{\rm Bj}$ are shown in Fig. 7, where they are compared to the NLO FFNS predictions from Fig. 2. The NNLO corrections do not exceed 10% and thus do not cover the differences between the FFNS A and FONLL-B theoretical predictions. Similar results are observed for cross sections as functions of other kinematic variables.

To better understand the differences between the FFNS and VFNS calculations, Fig.2*** which displays the cross section vs. Q^2 is particularly instructive. We see at low scales the FFNS and VFNS results coincide. When the μ scale is below the charm threshold scale (typically taken to be $\sim m_c$) the charm PDF vanishes and the FFNS and VFNS reduce to the same result.[2] For increasing scales, the VFNS resums the $\alpha_S \ln(\mu^2/m_c^2)$ contributions via the DGLAP evolution equations and the FFNS and VFNS will slowly diverge logarithmically. This behavior is observed in Fig.2*** and consistent with the characteristics demonstrated in Ref. [36].

More precisely, Ref. [36] used a matched set of $N_F = 3$ and $N_F = 5$ PDFs to study the impact of the scheme choice at large scales. They found the resummed contributions in the VFNS yielded a larger cross section than the FFNS (the specific magnitude was x-dependent), and that for Q scales more than a few times the quark mass, the differences due to scheme choice exceeded the differences due to (estimated) higher order contributions [36].

2.2 Contributions from different partonic subprocesses

[perhaps this text would be more appropriate in an earlier theory section] The reduced charm CC production cross sections can be expressed as a linear combinations of the structure functions:

$$\sigma^{\pm}_{\rm charm,CC} = 0.5(Y_+ F_2^{\pm} \mp Y_- x F_3^{\pm} - y^2 F_L^{\pm}), \qquad Y_{\pm} = 1 \pm (1-y)^2. \tag{1}$$

In the simplified Quark Parton Model, where gluons are not present, the structure functions become:

$$\begin{aligned} F_2^+ &= xD + x\overline{U}, \\ F_2^- &= xU + x\overline{D}, \\ F_L &= 0, \\ xF_3^+ &= xD - x\overline{U}, \\ xF_3^- &= xU - x\overline{D}. \end{aligned} \tag{2}$$

The terms xU, xD, $x\overline{U}$ and $x\overline{D}$ denote the sums of parton distributions for up-type and down-type quarks and anti-quarks, respectively. Below the b-quark mass threshold,

[2] Note that while the charm threshold scale μ_c is commonly set to the charm quark mass m_c, the choice of μ_c is arbitrary and amounts to a renormalzation scheme choice [35].

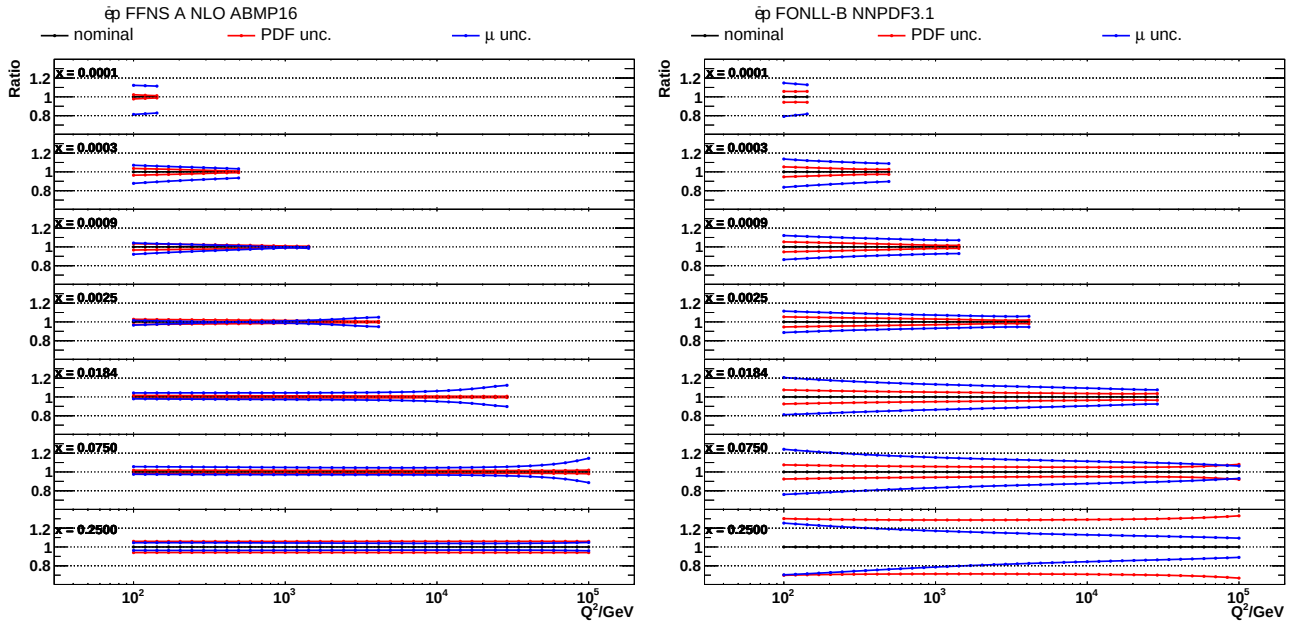

Figure 4 Relative theoretical uncertainties of charm CC predictions for the LHeC as a function of Q^2 for different values of x_{Bj} calculated in the FFNS A and FONLL-B schemes. The PDF and scale uncertainties are shown separately.

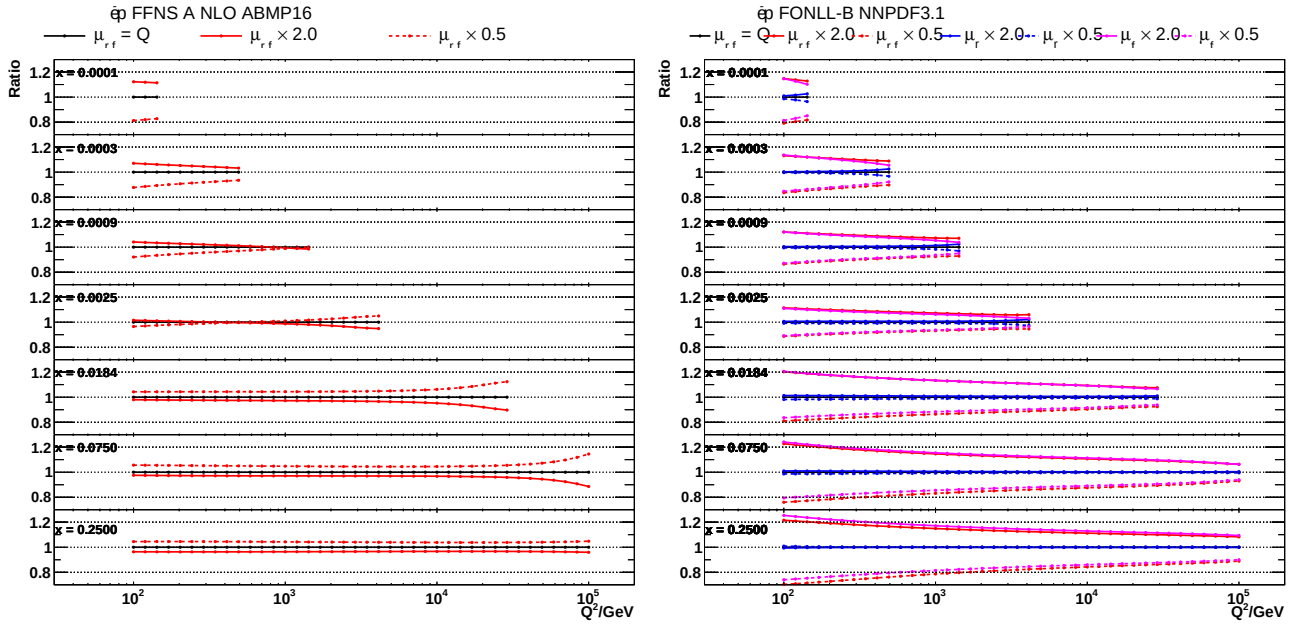

Figure 5 The impact of separate scale variations on charm CC predictions for the LHeC as a function of Q^2 for different values of x_{Bj} calculated in the FFNS A and FONLL-B schemes.

these sums are related to the quark distributions as follows:

$$\begin{aligned} xU &= xu + xc, \\ x\overline{U} &= x\bar{u} + x\bar{c}, \\ xD &= xd + xs, \\ x\overline{D} &= x\bar{d} + x\bar{s}. \end{aligned} \tag{3}$$

In the FFNS the charm quark density is zero. In the phase-space corners $y \to 0$ and $y \to 1$, the following asymptotics take place:

$$\begin{aligned} y \to 0 &: \sigma^{\pm}_{\mathrm{charm,CC}} = F_2^{\pm} = xD(x\overline{D}) + xU(x\overline{U}), \\ y \to 1 &: \sigma^{\pm}_{\mathrm{charm,CC}} = 0.5(F_2^{\pm} \mp xF_3^{\pm}) = xU(x\overline{U}). \end{aligned} \tag{4}$$

Thus the contribution from the strange quark PDF is suppressed at high y.

Figures 8, 9 and 10 show contributions from different partonic subprocesses for charm CC production cross sections in the FFNS A and FONLL-B schemes as a function

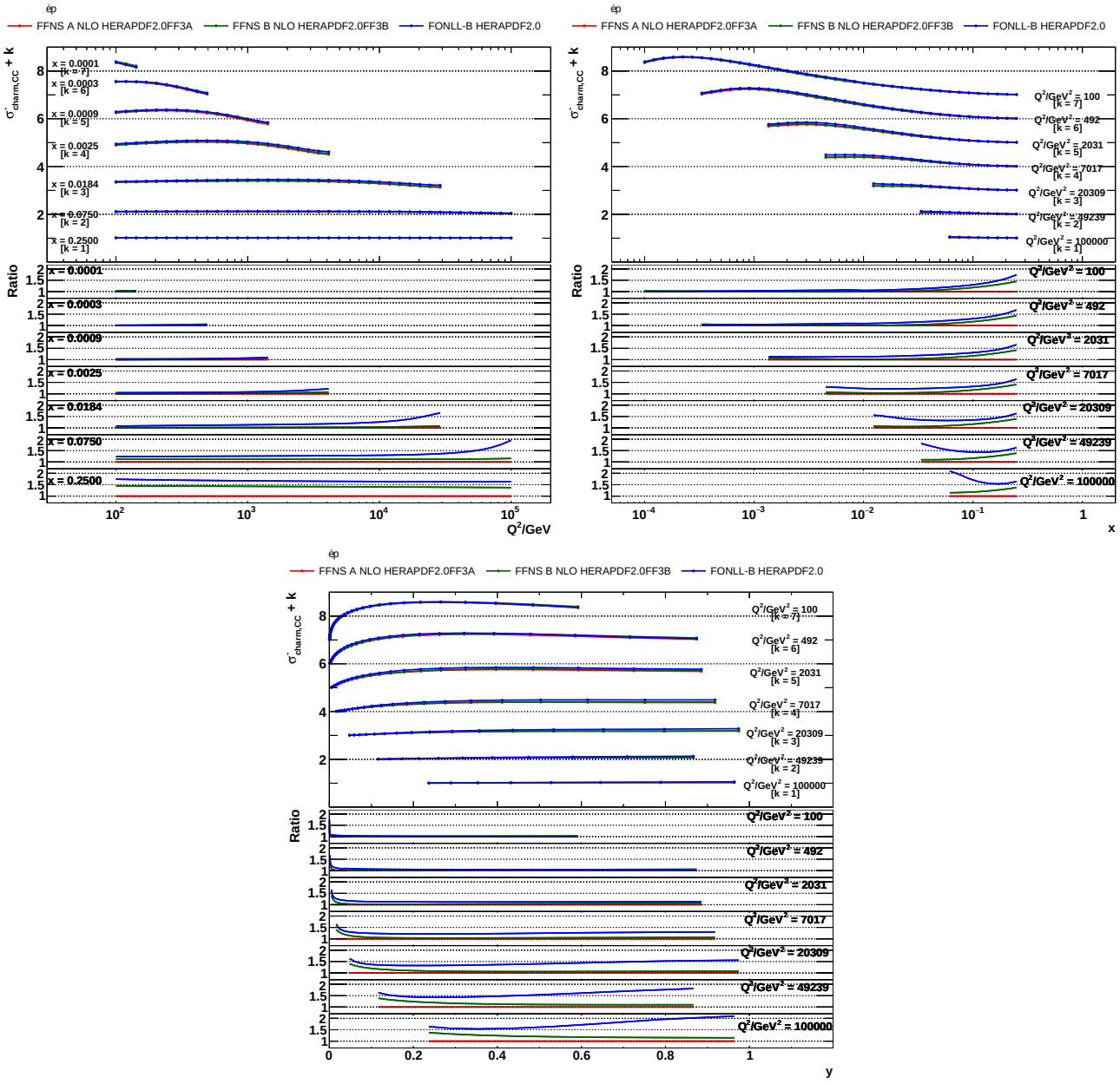

Figure 6 The theoretical predictions for charm CC production at the LHeC as a function of Q^2 (x_{Bj}, y) for different values of x_{Bj} (x_{Bj}, Q^2) obtained using the HERAPDF2.0 PDF sets in the FFNS A, FFNS B and FONLL-B schemes. The bottom panel display the theoretical predictions normalised to the nominal values of the FFNS A predictions.

of x_{Bj} for different values of Q^2, as a function of Q^2 for different values of x_{Bj}, and as a function of y for different values of Q^2, respectively. In both scheme, the strange quark PDF contributes only about 50% to total charm CC production. In particular, at high y its contribution drops to zero in favor of the gluon or charm quark PDF (see Fig. 10 and Eq. 4). Similar phenomena (although less pronounced) is observed at low x_{Bj} and/or high Q^2. In these phase space regions, the dominant contributions to the cross sections are the gluon PDF (in the FFNS) or the charm quark PDF (in the VFNS). Remarkably, these contributions as functions of Q^2, x_{Bj} and y behave qualitatively very similar in the FFNS and VFNS.

Figures 7,8,9*** display a particularly interesting pattern; the gluon contribution for the FFNS is strikingly similar to the charm contribution in the VFNS.

In the FFNS, the charm is produced predominantly from the explicit process $g\gamma \to c\bar{c}$. In contrast, for the VFNS the $g \to c\bar{c}$ splitting is implicit (internal to the proton and evolved with the DGLAP evolution equations); the charm parton then emerges from the proton to participate in the $c\gamma \to c$ process. The fundamental underlying process is the

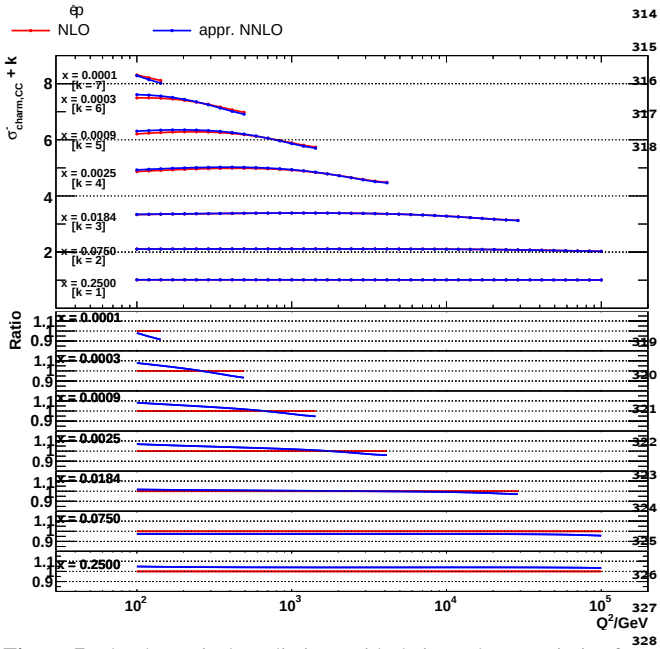

Figure 7 The theoretical predictions with their total uncertainties for charm CC production at the LHeC as a function of Q^2 for different values of x_{Bj} calculated in the FFNS A scheme at NLO and approximate NNLO. The bottom panel display the theoretical predictions normalised to the nominal values of the FFNS A NLO predictions.

same in both the FFNS and VFNS, but the factorization boundary between the PDF and the hard scattering cross section, $f \otimes \hat{\sigma}$, (determined by μ and the scheme choice) is different.[3]

3 PDF constraints from charm CC pseudodata

The impact of charm CC cross section measurements at the LHeC on the PDFs is quantitatively estimated using a profiling technique [37]. This technique is based on minimizing χ^2 between data and theoretical predictions taken into account both experimental and theoretical uncertainties arising from PDF variations. Two NLO PDF sets were chosen for this study: ABMP16 [30] and NNPDF3.1 [33] available via the LHAPDF interface (version 6.1.5) [38]. All PDF sets are provided with uncertainties in the format of eigenvectors.

For this study, pseudodata representing measurements of charm CC production cross sections as a function of Q^2 and x are used. **[TODO: describe how pseudodata were produced]** The study is performed using the XFITTER program (version 2.0.0) [39], an open-source QCD fit framework for PDF determination. The theoretical predictions are calculated at NLO QCD in the FFNS with the number of active flavours $n_f = 3$ and FONLL-B with $n_f = 5$. The running charm mass is set to $m_c(m_c) = 1.27$ GeV and α_s is set to the value used for the corresponding PDF extraction. The renormalisation and factorisation scales are chosen to be $\mu_{\mathrm{r}} = \mu_{\mathrm{f}} = Q^2$.

The χ^2 value is calculated as follows:

$$\chi^2 = \mathbf{R}^T \mathbf{Cov}^{-1} \mathbf{R} + \sum_{\beta} b^2_{\beta,\mathrm{th}}, \quad \mathbf{R} = \mathbf{D} - \mathbf{T} - \sum_{\beta} \Gamma_{\beta,\mathrm{th}} b_{\beta,\mathrm{th}}, \quad (5)$$

where $\mathbf{D}$ and $\mathbf{T}$ are the column vectors of the measured and predicted values, respectively, and the correlated theoretical PDF uncertainties are included using the nuisance parameter vector $\boldsymbol{b}_{\mathrm{th}}$ with their influence on the theory predictions described by $\Gamma_{\beta,\mathrm{th}}$, where index β runs over all PDF eigenvectors. For each nuisance parameter a penalty term is added to the χ^2, representing the prior knowledge of the parameter. No theoretical uncertainties except the PDF uncertainties are considered. The full covariance matrix representing the statistical and systematic uncertainties of the data is used in the fit. The statistical and systematic uncertainties are treated as additive, i.e., they do not change in the fit. The systematic uncertainties are assumed uncorrelated between bins.

To treat the asymmetric PDF uncertainties of the NNPDF3.1 set, the χ^2 function in Eq. 5 is generalised assuming a parabolic dependence of the prediction on the nuisance parameter [39]:

$$\Gamma_{\beta,\mathrm{th}} \rightarrow \Gamma_{\beta,\mathrm{th}} + \Omega_{\beta,\mathrm{th}} b_{\beta,\mathrm{th}}\,, \quad (6)$$

where $\Gamma_{\beta,\mathrm{th}} = 0.5(\Gamma^{+}_{\beta,\mathrm{th}} - \Gamma^{-}_{\beta,\mathrm{th}})$ and $\Omega_{\beta} = 0.5(\Gamma^{+}_{\beta,\mathrm{th}} + \Gamma^{-}_{\beta,\mathrm{th}})$ are determined from the shifts of predictions corresponding to up ($\Gamma^{+}_{\beta,\mathrm{th}}$) and down ($\Gamma^{-}_{\beta,\mathrm{th}}$) PDF uncertainty eigenvectors.

The values of the nuisance parameters at the minimum, $b^{\mathrm{min}}_{\beta,\mathrm{th}}$ are interpreted as optimised, or profiled, PDFs, while their uncertainties determined using the tolerance criterion of $\Delta\chi^2 = 1$ correspond to the new PDF uncertainties. The profiling approach assumes that the new data are compatible with theoretical predictions using the existing PDFs, such that no modification of the PDF fitting procedure is needed. Under this assumption, the central values of the measured cross sections are set to the central values of the theoretical predictions.

The original and profiled ABMP16 and NNPDF3.1 PDF uncertainties are shown in Figs. 11–14. The uncertainties of the PDFs are presented at the scales $\mu^2_{\mathrm{f}} = 100$ GeV^2 and $\mu^2_{\mathrm{f}} = 100000$ GeV^2. A strong impact of the charm CC pseudodata on the PDFs is observed for both PDF sets. In particular, the uncertainties of the strange PDF are strongly reduced once the pseudodata are included in the fit. Also the gluon PDF uncertainties are decreased. Furthermore, in the case of the NNPDF3.1 set and FONLL scheme, the charm PDF uncertainties are reduced significantly.

[3] Note there is a "subtraction" term ($g \rightarrow c\bar{c} \otimes c\gamma \rightarrow c$) which closely matches the LO $c\gamma \rightarrow c$ process, but this $\mathcal{O}(\alpha\,\alpha_S)$ process is contained in the NLO gluon-initiated contribution.

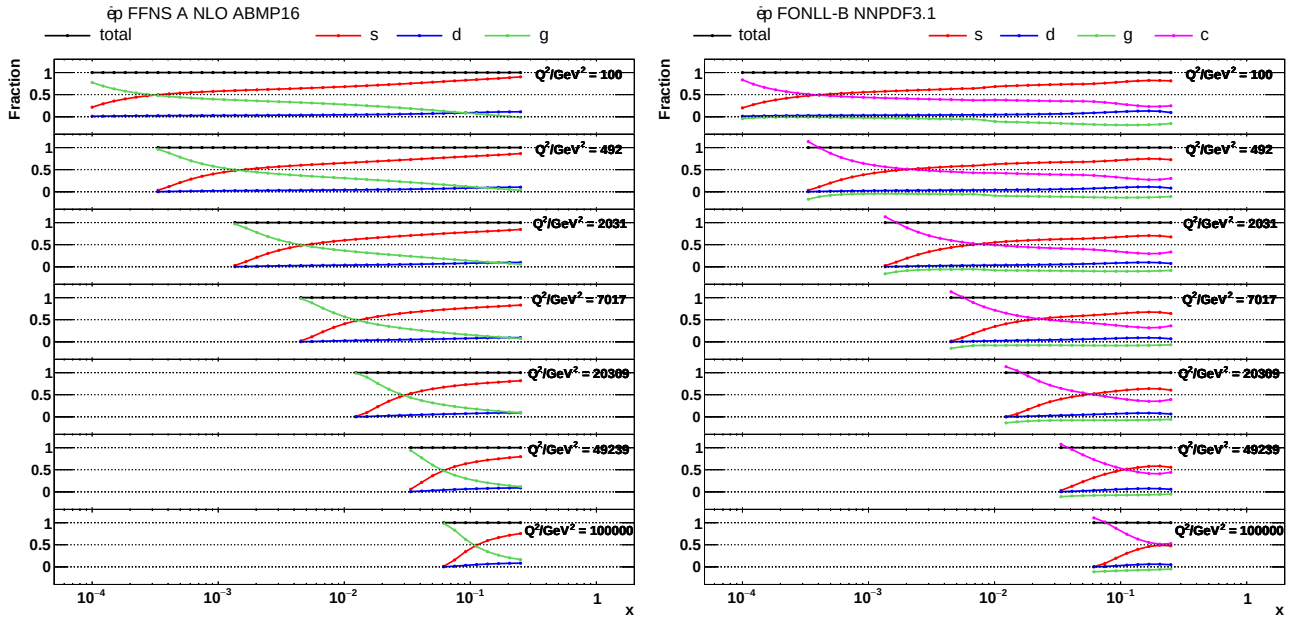

Figure 8 The partonic subprocesses for charm CC production cross sections in the FFNS A (left) and FONLL-B (right) schemes as a function of x_{Bj} for different values of Q^2.

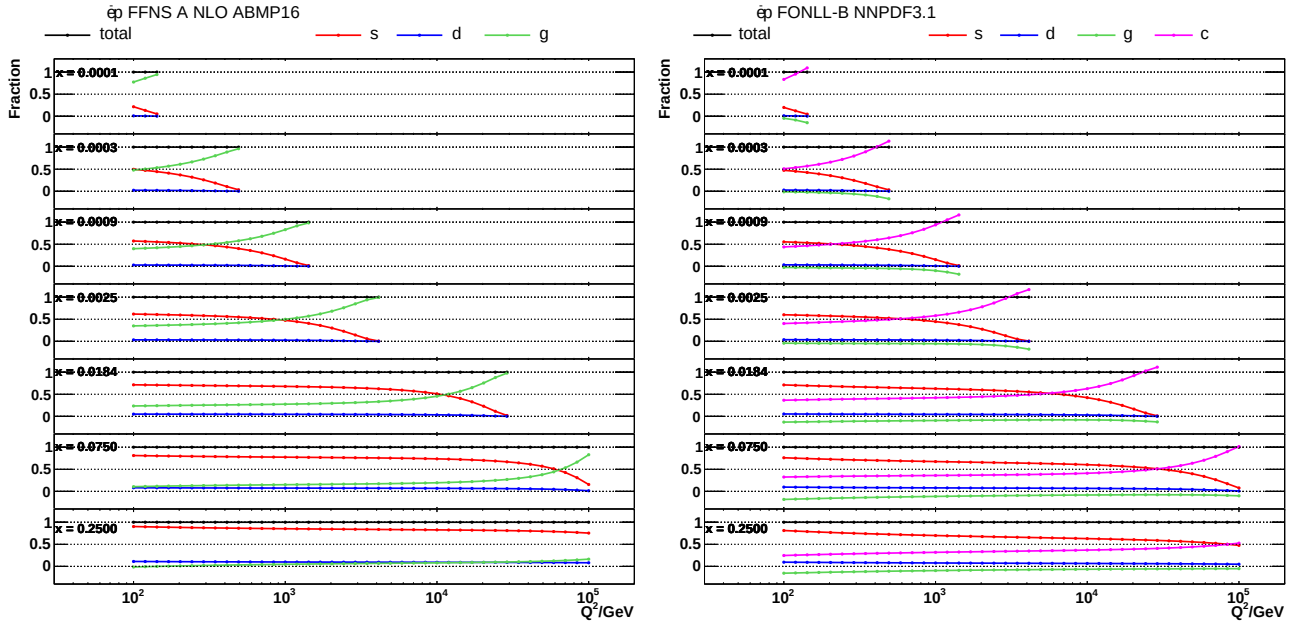

Figure 9 The partonic subprocesses for charm CC production cross sections in the FFNS A (left) and FONLL-B (right) schemes as a function of Q^2 for different values of x_{Bj}.

4 Discussion and summary

Acknowledgements We would like to thank John C. Collins, Aleksander Kusina, Ted C. Rogers, Ingo Schienbein, George Sterman, ... for useful discussion.

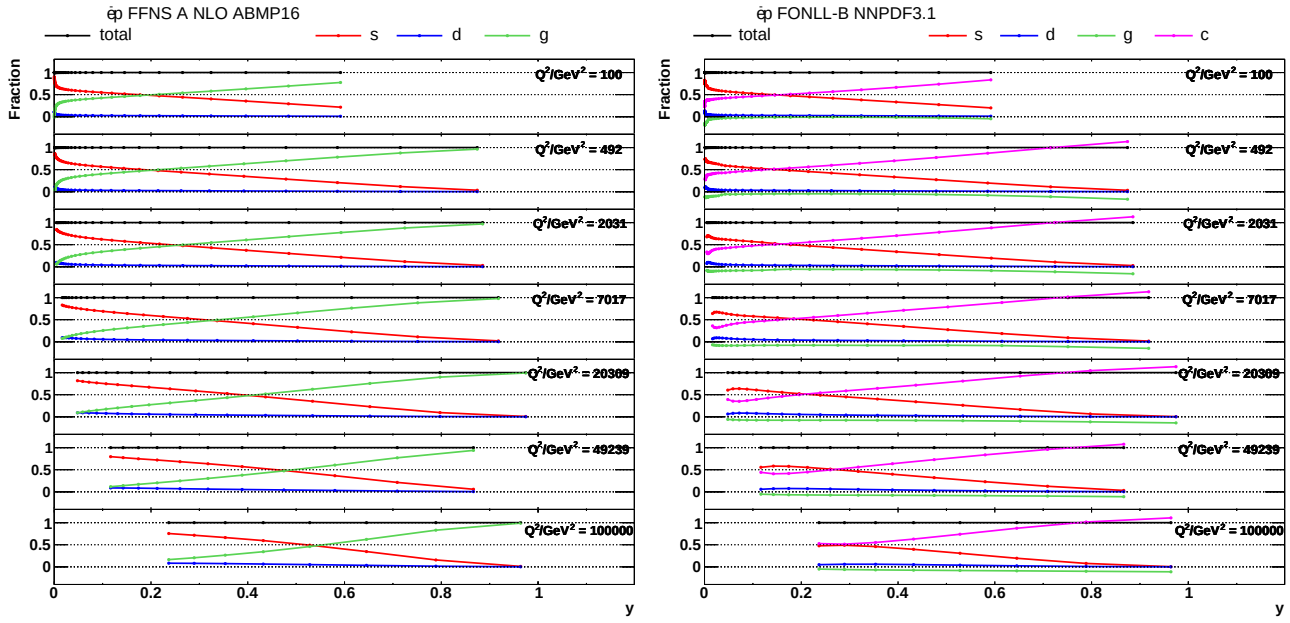

Figure 10 The partonic subprocesses for charm CC production cross sections in the FFNS A (left) and FONLL-B (right) schemes as a function of y for different values of Q^2.

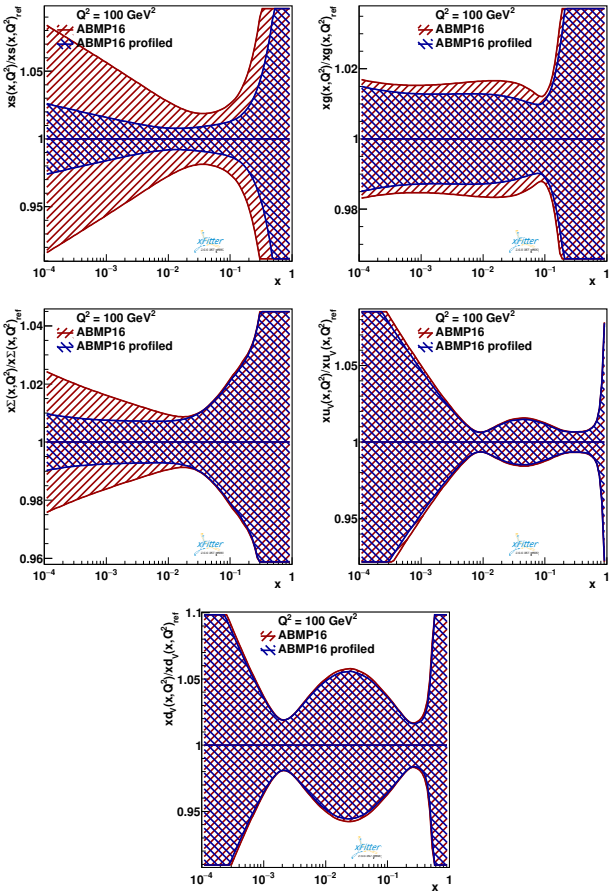

Figure 11 The relative strange (top left), gluon (top right), sea quark (middle left), u valence quark (middle right) and d valence quark (bottom) PDF uncertainties at $\mu_f^2 = 100$ GeV^2 of the original and profiled ABMP16 PDF set.

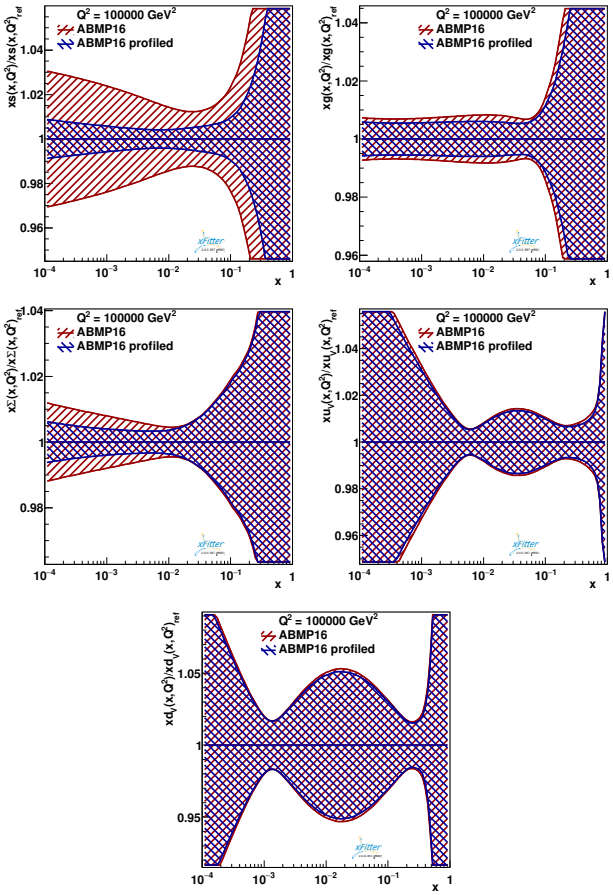

Figure 12 The relative strange (top left), gluon (top right), sea quark (middle left), u valence quark (middle right) and d valence quark (bottom) PDF uncertainties at $\mu_f^2 = 100000$ GeV^2 of the original and profiled ABMP16 PDF set.

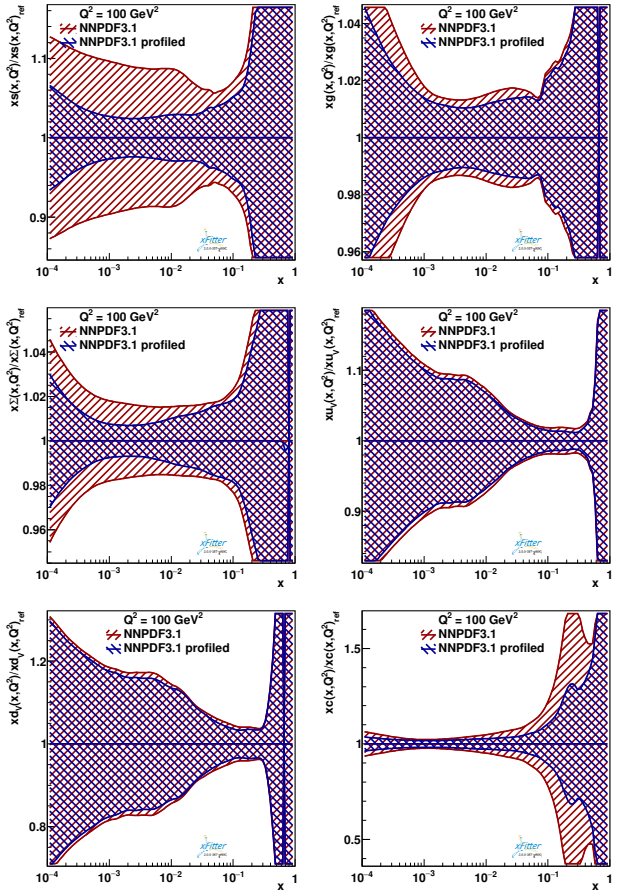

Figure 13 The relative strange (top left), gluon (top right), sea quark (middle left), u valence quark (middle right), d valence quark (bottom left) and charm quark (bottom right) PDF uncertainties at $\mu_f^2 = 100$ GeV^2 of the original and profiled NNPDF3.1 PDF set.

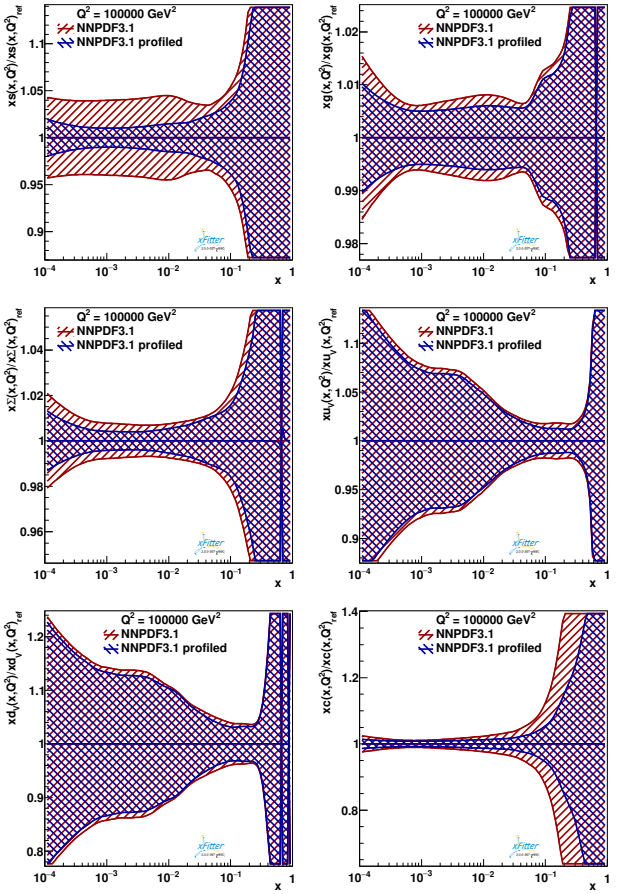

Figure 14 The relative strange (top left), gluon (top right), sea quark (middle left), u valence quark (middle right), d valence quark (bottom left) and charm quark (bottom right) PDF uncertainties at $\mu_f^2 = 100000$ GeV^2 of the original and profiled NNPDF3.1 PDF set.

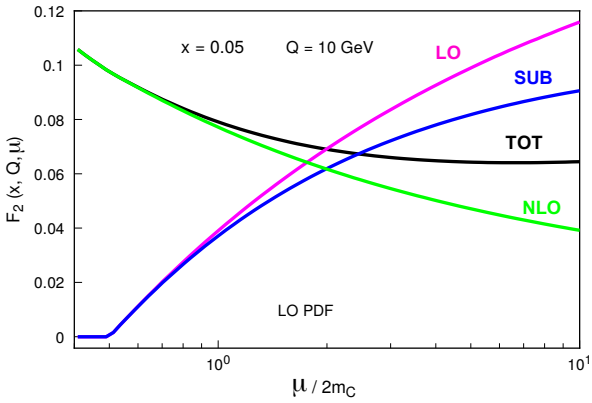

Figure 15 Calculation of F_2^c vs. μ in the VFNS illustrating the cancellation of the LO ($\bar{c}W^+ \to \bar{s}$) and the SUB ($g \to \bar{c}$)$\otimes$($\bar{c}W^+ \to \bar{s}$) contributions in the region $\mu \sim m_c$. The Q scale is fixed at 10 GeV and the charm PDF is matched at $\mu_c = m_c$ such that $f_c(x, \mu = m_c) = 0$.

TO DO LIST: * Follow up on John Collins' list [MOSTLY DONE] * Add brief mention at end that this applies also to bottom quark [at end] * refs from Sasha: LHC W+c measurements: [40–42]

Appendix A: F_2^{charm} Beyond Leading-Order

The Multi-Scale Problem: The charged current DIS charm production process involves some interesting issues that we will explore here in detail. In particular, there are multiple mass and energy scales which span a wide kinematic range, and it becomes an intricate puzzle to treat them all properly.

For this current illustration, we will focus on the contribution to the DIS F_2^c structure function from the process involving the strange and charm quark; other quark combinations can be addressed in a similar manner. In particular, we will show that as we go to higher-orders the F_2^c structure function must be defined carefully so that i) theoretically it is free of divergences and independent of the renormalization scales, and ii) experimentally it matches what is measured by the detector.

Overview:

... to be filled in ... (what other detailed are needed???)

The Mass Scales: There are four mass scales that enter this process: $\{Q, \mu, m_s, m_c\}$; additionally, in the case of the VFNS we have the matching scale, μ_c.

The Q scale is the invariant mass of the virtual boson probe (W^+ in this case), and can be related to the energy and angle of lepton; this is a physically measurable kinematic variable.

In contrast, the renormalization scale μ is an unphysical scale used to factorize the PDF and the hard scattering cross section; thus, the physics should be insensitive to a variation of μ. As our calculations typically involve the dimensionless combination $\ln(\mu^2/Q^2)$, we generally choose $\mu \sim Q$ avoid large logarithms.

The strange quark is a "light" active parton with an associated PDF $s(x)$ and mass m_s. The strange quark mass is comparable or less than other hadronic scales which are neglected; as such, it serves only as a regulator and plays no physical role, and we can take $m_s \to 0$ if we choose.

The charm quark is a "heavy" object; its associated mass m_c does play a physical role and cannot be neglected. There may or may not be a PDF associated with the charm. In a 3-flavor FFNS scheme, there is no charm PDF. In a 4-flavor VFNS there is a charm PDF only when the μ scale is above the scale where the charm PDF is activated; we call this the matching scale, μ_c. It is common[4] to set $\mu_c = m_c$, but this is not required.[5] In this study we will fix the matching scale to this common choice: $\mu_c = m_c$.

What makes this process complex is there is no fixed hierarchy for the mass scales, and we will need to compute both in the low Q region where $Q \lesssim m_c$ as well as the high Q region $Q \gg m_c$.

Because there are two different quark masses $\{m_s, m_c\}$ involved in the charged current DIS flavor-changing process, we can examine the mass singularities of the t-channel and u-channel separately. This separation is particularly useful to understand how the individual mass singularities are addressed, and how FFNS and VFNS organize the contributions to the total structure function.

3-Flavor FFNS: To be specific, we will consider charged-current DIS production of a charm quark. We first compute this in a 3-flavor (FFNS) scheme where $\{u, d, s\}$ are light "active" partons in the proton, and charm $\{c\}$ is considered an external "heavy" particle. This can be implemented in the ACOT scheme[45] for example by using a CWZ renormalization[46] where the light "active" partons are renormalized with normal $\overline{MS}$, and the "heavy" quarks use a zero-momentum subtraction. In this scheme, the **leading-order** (LO) process is $sW^+ \to c$ as illustrated in Fig. 15. At **next-to-leading-order** (NLO), we then include $gW^+ \to c\bar{s}$ which has both t-channel and u-channel contributions.[6]

[4] The choice of matching scale $\mu_c = m_c$ is common because at NLO the $\overline{MS}$ matching conditions on the PDFs are proportional to the DGLAP kernel times $\ln(\mu/m_c)$, as explicit calculation shows the constant term vanishes; thus we have the simple boundary condition $f_c(x, \mu = m_c) = 0$. At NNLO, the constant term is non-zero and this yields $f_c(x, \mu = m_c) \neq 0$. See [43] and references therein.

[5] By displacing the matching scale to larger values $\mu_c \gg m_c$, can have the advantage of avoiding delicate cancellations in the region $\mu \sim m_c$; this flexibility was explored in Refs. [35, 44] .

[6] Note, there are also corresponding quark-initiated processes; we will focus on the gluon-initiated processes as this is sufficient to illustrate our points. Both the gluon- and quark-initiated contributions are included in our calculations.

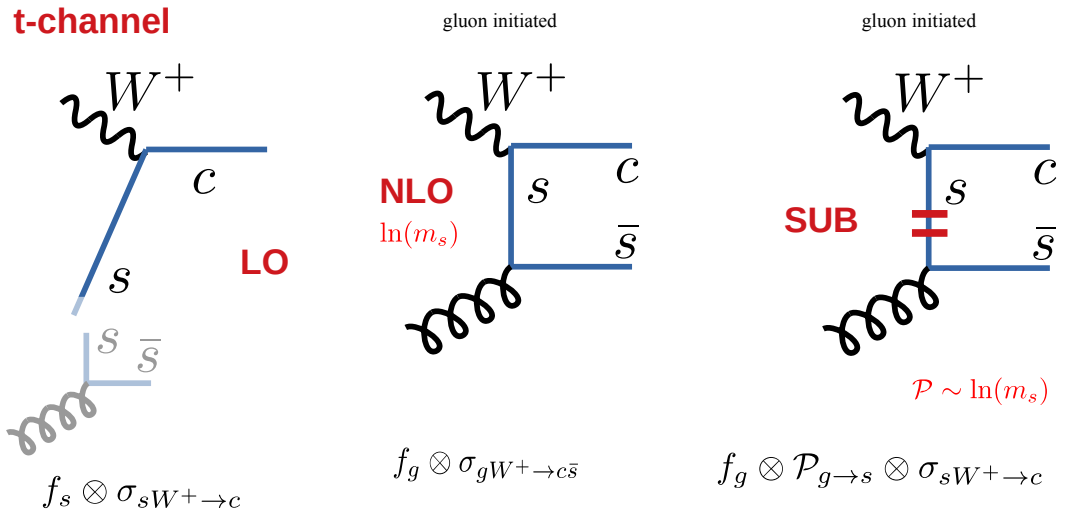

Figure 16 Gluon t-channel processes up to $\mathcal{O}(\alpha_S^1)$.

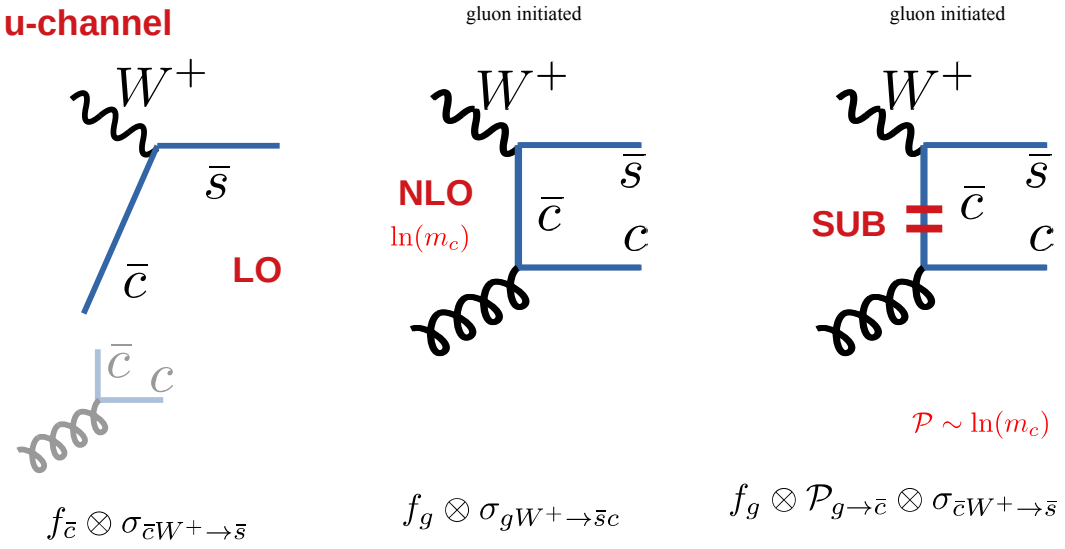

Figure 17 Gluon NLO u-channel processes up to $\mathcal{O}(\alpha_S^1)$.

***t*-Channel:** The t-channel process has an intermediate s-quark exchanged, and if we use the strange quark mass m_s to regulate the singularities, this will yield a contribution proportional to $\ln(Q/m_s)$. This mass singularity arises from the region of phase space where the exchanged s-quark becomes collinear and close to the mass-shell; that is, when the phase space of the $gW^+ \to c\bar{s}$ process begins to overlap with that of the $sW^+ \to c$ process. This "double counting" is resolved by a **subtraction** (SUB) counter-term given by:

$$(SUB) \sim f_g \otimes \widetilde{f}_{g\to s} \otimes \sigma_{sW^+\to c} \quad .$$

Here, $\widetilde{f}_{g\to s}$ is the perturbative splitting of the gluon into an $s\bar{s}$ pair; the leading term is proportional to:[7]

$$\widetilde{f}_{g\to s}(x,\mu) \sim \frac{\alpha_S(\mu)}{2\pi} P^{(1)}_{g\to s}(x) \ln\left(\frac{\mu^2}{m_s^2}\right) + \mathrm{O}(\alpha_s^2)$$

where $P^{(1)}_{g\to s}(x)$ is the α_S^1 DGLAP splitting kernel for $g \to s$.

The complete contribution to the structure function is given by:

$$F_2^c \sim TOT = LO + (NLO - SUB)$$

The complete $\mathcal{O}(\alpha_s^1)$ contribution is the combination $(NLO - SUB)$; our separation into NLO and SUB is simply to illustrate the interplay of these components. Both the

[7] The scale of the SUB term is μ as the relevant scale here is the renormalization scale of the PDF: $f(x,\mu) \otimes \hat{\sigma}(x,Q,\mu)$.

NLO and SUB terms have $\ln(m_s)$ divergences, but these precisely cancel and yield a well defined result even as we take the $m_s \to 0$ limit.[8]

u-Channel: We next examine the u-channel NLO contribution to the $gW^+ \to c\bar{s}$ process. This has an intermediate c-quark exchanged, and is proportional to $\ln(Q/m_c)$. In the FFNS where the charm is a "heavy" non-parton, there is no counter-term for this graph, and the resulting observables will retain the $\ln(Q/m_c)$ dependence. In principle, this means when we go to large Q-scales, these terms will begin to degrade the convergence of our perturbation series. In practice, while this degradation only grows logarithmically, at large scales (such as at the LHC) we do find it convenient to treat the charm on an equal-footing as the u,d,s partons.

4-Flavor VFNS: We now turn to the 4-flavor (VFNS) scheme where we include the charm quark as an "active" parton and compute its associated PDF.

In this case, there is a u-channel counter-term (SUB) given by $f_g \otimes \widetilde{f}_{g\to\bar{c}} \otimes \sigma_{\bar{c}W^+\to\bar{s}}$ which is proportional to $\ln(\mu/m_c)$. The NLO u-channel contribution will have a $\ln(Q/m_c)$ contribution, so the combination $(NLO-SUB)$ is also free of mass singularities.[9]

What is less obvious is that we also must include the LO process $\bar{c}W^+ \to \bar{s}$. There are two ways we can understand why this is necessary.

Explanation #1: Matching of LO and SUB: Recall that in the t-channel case, the subtraction term SUB removed the double counting between the LO $sW^+ \to c$ and NLO $gW^+ \to c\bar{s}$ processes.

The u-channel case is analogous in that this subtraction term removes the double counting between the LO $\bar{c}W^+ \to \bar{s}$ and NLO $gW^+ \to c\bar{s}$ processes; both contributions are required to ensure the resulting cross section is insensitive to the μ-scale.

This is apparent in Fig. 15 where we plot the individual terms versus the μ scale for a fixed x and Q. In the region of $\mu \sim m_c$, the charm PDF $f_c(x,\mu)$ (and hence, the LO contribution) rises very quickly as the DGLAP evolution is driven by the very large gluon via $g \to c\bar{c}$ splitting, and combined with a large $\alpha_S(\mu)$. The SUB subtraction also rises quickly as this is driven by the logarithmic term $\ln(\mu^2/m_c^2)$. The difference $(LO-SUB)$ is the physical contribution to the total $[TOT = LO+NLO-SUB]$, and it is this combination which is smooth across the "turn on" of the charm PDF at the matching scale $\mu_c = m_c$. We now see that if we neglect the LO ($\bar{c}W^+ \to \bar{s}$) contribution, we lose the cancellation between LO and SUB in the region $\mu \sim m_c$, and our structure function (or cross section) would have an anomalous shift at the arbitrarily location (μ_c) where we turn on the charm PDF.

As we vary the unphysical renormalization scale μ, we are simply shifting contributions between the separate $\{LO, NLO, SUB\}$ terms which individually exhibit a large μ-dependence. However, the total combination (TOT) which represents the physical observable is relatively insensitive to μ (up to higher orders), and this property is evident in Fig. 15.

Explanation #2: Removing "Double Counting:" A second way to understand why we require the LO process $\bar{c}W^+ \to \bar{s}$ is to consider the regions of phase space covered by each of the sub-processes. The singularity of the u-channel NLO $gW^+ \to c\bar{s}$ processes arises the phase space region when the intermediate $\bar{c}$ quark becomes collinear and close to the mass-shell.[10] This is precisely the phase space region of the LO process $\bar{c}W^+ \to \bar{s}$ where the partonic $\bar{c}$-quark is collinear to the hadron. The SUB term then removes the "double counting" between the LO and NLO contributions; hence, all three contributions $\{LO, NLO, SUB\}$ are necessary to cover the full phase space.

This is also apparent if we consider the transverse momentum (p_T) of the final-state charm in the Breit frame. For the LO $\bar{c}W^+ \to \bar{s}$ process in the Breit frame, the incoming W^+ and $\bar{c}$ are collinear, and the produced $\bar{s}$ must have zero p_T in this frame.

For the NLO $gW^+ \to c\bar{s}$ process, we integrate over the complete phase space for the exchanged $\bar{c}$ quark, and this will include the region where the $\bar{c}$ quark is emitted nearly collinear to the gluon and nearly on-shell; in this region the $\bar{c}$ quark will have $p_T \sim 0$ and we encounter a singularity from the internal $\bar{c}$ propagator. The $p_T \sim 0$ region is precisely that subtracted by the SUB counter term,[11] and this ensure that the combination $(NLO-SUB)$ is free of divergences.

Recap: To recap, i) the combination of the LO and SUB terms ensure a minimal μ-variation at low μ scales, and ii) the combination of SUB and NLO ensure the mass singularities are canceled at high μ scales.

This interplay of the terms illustrates some of the intricacies of QCD, especially since this exchange is across different orders of α_s.

Furthermore, note that in the u-channel for both the LO and SUB contributions, the charm quark is collinear with the incoming hadron, and thus exits in the hadron remnants.

[8] In fact, we could have taken $m_s = 0$ initially and used dimensional regularization to compute the contributions.

[9] Specifically, the combination $(NLO-SUB)$ is free of mass singularities and finite in the limit $m_c \to 0$. Note, the VFNS fully retains the charm quark mass m_c and (in contrast to some claims in the literature) the factorization holds up to $\mathcal{O}(\Lambda^2/Q^2)$ corrections; all terms of order (m_c^2/Q^2) are fully included.[47]

[10] Specifically, the charm quark is off-shell by the order of its mass m_c; this is independent of the scale Q and ***does not*** assume any $Q \gg m_c$ limit.

[11] Specifically, the incoming W^+ and g are collinear, and the gluon then emits a collinear $c\bar{c}$ pair so the final $\bar{s}$ has zero p_T.

While this may be experimentally unobservable, because we are asking for a *"fully inclusive"* F_2^c, these contributions cannot be simply ignored. We will discuss this further in the following section.

Defining F_2^c: The u-channel LO $\bar{c}W^+ \to \bar{s}$ process foreshadows difficulties we encounter if we try and extend the concept of a "fully inclusive" F_2^c to higher orders. We note that in Ref. [47] Collins extended the proof of factorization to include heavy quarks such as charm and bottom for an inclusive structure function F_2; there is no corresponding proof for an *"fully inclusive"* F_2^c because a well defined F_2^c that is free of singularities will depend on experimental cuts or theoretical regulators. The simplistic definition that F_2^c is the contribution to F_2 from states with charm in the final state is not appropriate.

The F_2^c that is measured experimentally is a differential cross section for producing a charm quark in the final state in a fiducial region; as we go to higher orders, we must be careful how we define this quantity so that it is singularity-free and μ-independent.

To characterize the problems in constructing a *"fully inclusive"* F_2^c, we can imagine starting from the (well defined) inclusive F_2, and then dividing the contributions into two sets: one for F_2^c for the "heavy" charm quark, and the rest into $F_2^{u,d,s}$ for the "light" quarks. We will show this division cannot be performed unambiguously.

The u-channel LO $\bar{c}W^+ \to \bar{s}$ process does not have any "apparent" charm quark in the final state, but this contribution is essential to balance with the SUB process $f_g \otimes \widetilde{f}_{g\to\bar{c}} \otimes \sigma_{\bar{c}W^+\to\bar{s}}$. Note that for the SUB process, the charm quark arises from a gluon splitting into a collinear $c\bar{c}$ pair which is then part of the hadron remnants. For the LO process, presumably our $\bar{c}$ quark also came from a gluon splitting into a collinear $c\bar{c}$ pair. Thus, if we want to define a *"fully inclusive"* F_2^c, it seems we must include those cases where the charm in contained in the hadron remnants.

This issues touches on the fact that because the charm parton is not observable, ultimately we must produce a charm meson (typically a D^*) via a fragmentation process. This requires the introduction of a set of fragmentation functions (FFs) which are scale-dependent and will factorize final-state singularities in a similar manner as the PDFs factor the initial-state singularities.[12] The attempt to define a *"fully inclusive"* F_2^c is further complicated by the fact that the FFs can produce a D* from the fragmentation of a gluon or a light hadron.

The Bubble Diagram:

Such difficulties of defining a *"fully inclusive"* F_2^c are not unique to the VFNS, and also are encountered in the FFNS. This is succinctly illustrated in Fig. 18 which shows a higher-order DIS process with a quark–anti-quark loop. Let us compute this diagram in a 3-flavor FFNS where the internal loop is a $c\bar{c}$-pair, and the external quark is a light $\{u,d,s\}$. If the final-state is represented by Cut-A, then we have charm quarks in the final state, and this should be included in F_2^c.

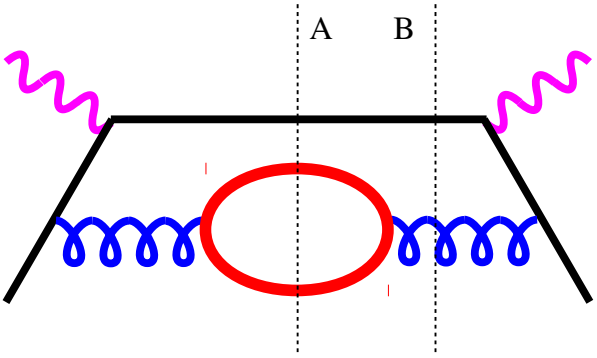

Figure 18 A higher order Feynman graph illustrating the difficulty in defining a "fully inclusive" F_2^{charm}. A light quark (q) scatters from a vector boson (V) with a $c\bar{c}$ in the internal loop. If we cut the amplitude at "A" we have charm in the final state and this must be included in F_2^{charm}. If we cut the amplitude with cut "B" there is no charm in the final state, but this process is required to cancel the divergences. Additionally, since this diagram contributes to the beta function, this highlights the complications of using an α_S and hard scattering $\hat{\sigma}$ with differing $N_{\rm eff}$.

However, if we instead use Cut-B as the final state, there is no charm in the final state, so this should not be included in F_2^c. [More precisely, when we renormalize the charm loop with zero-momentum subtraction, this contribution effectively decouples.] Thus, the contribution from Cut-A will be included in F_2^c, but the contribution from Cut-B will not.

If we had included the contributions for both Cut-A and Cut-B, the total would be free of divergences. The QED analog of this is the well known Block-Nordsieck theorem,[48] and the QCD extensions were performed by Libby and Sterman.[49, 50] For example, the bubble diagram of Fig. 18 is encountered in the F_2^c heavy quark calculations of Refs. [51, 52]; here, an additional scale Δ must be introduced to cut on the invariant mass of the internal quark–anti-quark pair and regulate the singularities.

The running α_S in the FFNS: The bubble diagram of Fig. 18 also highlights the difficulty of using a $N_{\rm eff} = 3$ FFNS with an $N_{\rm eff} = 4$ flavor running $\alpha_S(\mu)$. In a $N_{\rm eff} = 3$ FFNS, internal $c\bar{c}$ loops decouple from the theory and are not included in the calculation; however, the $N_{\rm eff} = 4$ β-function requires precisely these $c\bar{c}$ loop contributions.[13] Once again, we cannot unambiguously divide the inclusive F_2 into separate "light" and "heavy" quantities.

[12] Also note, for the NLO quark-initiated contributions (not shown) we will have final state singularities from processes such as $c \to cg$ which will be factorized into the fragmentation functions.

[13] Note; this deficiency can in principle be patched order-by-order by expanding the β-function and inserting the required terms at each order [53–55].

Extensions to bottom and top: While we have used the charm quark to illustrate these features, the same properties can, in principle, be applied to both the bottom and top quark.[14] For the case of the bottom quark, the larger mass m_b yields a smaller $\alpha_s(\mu)$ for $\mu \sim m_b$ and the evolution of $f_b(x,\mu)$ is thus reduced; nevertheless, for large scale processes (such as the LHC) we often find it convenient to make use of $f_b(x,\mu)$ and treat the 5-flavors on an equal footing. For the case of the top quark, the very large mass m_t yields a much smaller $\alpha_s(\mu)$ for $\mu \sim m_t$ and the evolution of $f_t(x,\mu)$ is comparatively reduced.

Summary

To properly define an F_2^c at all orders, we must be careful to match the theoretical quantity to what is actually measured experimentally. This is more complex than simply asking for the portion of F_2 which has charm in the final state, and is an issue for both the FFNS and VFNS. The experimental F_2^c is a differential cross section for producing a charm meson in a fiducial region; this physical observable is singularity-free and μ-independent.

We can compute in the FFNS, but in the large energy limit, we encounter $\ln(Q^2/m_c^2)$ divergences and this, in part, contributes to the observed differences at large Q scales.

The VFNS includes the charm quark as an active parton for μ scales above a matching scale μ_c. For large Q scales, the mass singularities of NLO and SUB will cancel to yield a result free of divergences. For scales $\mu \sim m_c$, cancellation between the LO and SUB contributions ensures minimal μ dependence; however, as this can be delicate to implement numerically, we have the option of displacing the matching scale μ_c to a larger scale where the cancellation is more stable.[35, 44]

References

1. H. Abdolmaleki, et al., Eur. Phys. J. **C78**(8), 621 (2018). DOI 10.1140/epjc/s10052-018-6090-8
2. H. Abramowicz, et al., Eur. Phys. J. **C75**(12), 580 (2015). DOI 10.1140/epjc/s10052-015-3710-4
3. J. Gao, L. Harland-Lang, J. Rojo, arXiv:1709.04922 (2017)
4. O. Behnke, A. Geiser, M. Lisovyi, Prog. Part. Nucl. Phys. **84**, 1 (2015). DOI 10.1016/j.ppnp.2015.06.002
5. O. Zenaiev, Eur. Phys. J. **C77**(3), 151 (2017). DOI 10.3204/PUBDB-2017-01474,10.1140/epjc/s10052-017-4620-4
6. H. Abdolmaleki, A. Khorramian, A. Aleedaneshvar, Nucl. Part. Phys. Proc. **282-284**, 27 (2017). DOI 10.1016/j.nuclphysbps.2016.12.006
7. E. Laenen, S. Riemersma, J. Smith, W.L. van Neerven, Nucl. Phys. **B392**, 162 (1993). DOI 10.1016/0550-3213(93)90201-Y
8. E. Laenen, S. Riemersma, J. Smith, W.L. van Neerven, Nucl. Phys. **B392**, 229 (1993). DOI 10.1016/0550-3213(93)90202-Z
9. T. Gottschalk, Phys. Rev. **D23**, 56 (1981). DOI 10.1103/PhysRevD.23.56
10. M. Gluck, S. Kretzer, E. Reya, Phys. Lett. **B398**, 381 (1997). DOI 10.1016/S0370-2693(97)90016-2, 10.1016/S0370-2693(97)00232-3. [Erratum: Phys. Lett.B405,392(1997)]
11. J. Blumlein, A. Hasselhuhn, P. Kovacikova, S. Moch, Phys. Lett. **B700**, 294 (2011). DOI 10.1016/j.physletb.2011.05.007
12. S. Alekhin, J. Blumlein, L. Caminadac, K. Lipka, K. Lohwasser, S. Moch, R. Petti, R. Placakyte, Phys. Rev. **D91**(9), 094002 (2015). DOI 10.1103/PhysRevD.91.094002
13. E.L. Berger, J. Gao, C.S. Li, Z.L. Liu, H.X. Zhu, Phys. Rev. Lett. **116**(21), 212002 (2016). DOI 10.1103/PhysRevLett.116.212002
14. A. Behring, J. BlÃŒmlein, A. De Freitas, A. Hasselhuhn, A. von Manteuffel, C. Schneider, Phys. Rev. **D92**(11), 114005 (2015). DOI 10.1103/PhysRevD.92.114005
15. V.M. Abazov, et al., Phys. Lett. **B743**, 6 (2015). DOI 10.1016/j.physletb.2015.02.012
16. H.L. Lai, P.M. Nadolsky, J. Pumplin, D. Stump, W.K. Tung, C.P. Yuan, JHEP **04**, 089 (2007). DOI 10.1088/1126-6708/2007/04/089
17. W.G. Seligman, et al., Phys. Rev. Lett. **79**, 1213 (1997). DOI 10.1103/PhysRevLett.79.1213
18. M. Tzanov, et al., Phys. Rev. **D74**, 012008 (2006). DOI 10.1103/PhysRevD.74.012008
19. G. Onengut, et al., Phys. Lett. **B632**, 65 (2006). DOI 10.1016/j.physletb.2005.10.062
20. J.P. Berge, et al., Z. Phys. **C49**, 187 (1991). DOI 10.1007/BF01555493
21. O. Samoylov, et al., Nucl. Phys. **B876**, 339 (2013). DOI 10.1016/j.nuclphysb.2013.08.021
22. A. Airapetian, et al., Phys. Lett. **B666**, 446 (2008). DOI 10.1016/j.physletb.2008.07.090
23. T. Aaltonen, et al., Phys. Rev. Lett. **100**, 091803 (2008). DOI 10.1103/PhysRevLett.100.091803
24. V.M. Abazov, et al., Phys. Lett. **B666**, 23 (2008). DOI 10.1016/j.physletb.2008.06.067
25. S. Kretzer, H.L. Lai, F.I. Olness, W.K. Tung, Phys. Rev. **D69**, 114005 (2004). DOI 10.1103/PhysRevD.69.114005

[14] Additionally, Collins specifically addressed the case of multiple heavy quarks which can allow for both charm and bottom in a unified framework; in contrast to some incorrect claims in the literature, there is no difficulty including multiple heavy quarks. (C.f, Ref. [47], Sec. IX.)

26. A.D. Martin, R.G. Roberts, W.J. Stirling, R.S. Thorne, Phys. Lett. **B604**, 61 (2004). DOI 10.1016/j.physletb.2004.10.040
27. M. Aaboud, et al., Eur. Phys. J. **C77**(6), 367 (2017). DOI 10.1140/epjc/s10052-017-4911-9
28. A.D. Martin, W.J. Stirling, R.S. Thorne, G. Watt, Eur. Phys. J. **C63**, 189 (2009). DOI 10.1140/epjc/s10052-009-1072-5
29. S. Alekhin, J. Blümlein, S. Moch, R. Placakyte, Phys. Rev. **D96**(1), 014011 (2017). DOI 10.1103/PhysRevD.96.014011
30. S. Alekhin, J. Blümlein, S. Moch, Eur. Phys. J. **C78**(6), 477 (2018). DOI 10.1140/epjc/s10052-018-5947-1
31. S. Alekhin. "openqcdrad". URL http://www-zeuthen.desy.de/~alekhin/OPENQCDRAD/
32. V. Bertone, S. Carrazza, J. Rojo, Comput. Phys. Commun. **185**, 1647 (2014). DOI 10.1016/j.cpc.2014.03.007
33. R.D. Ball, et al., Eur. Phys. J. **C77**(10), 663 (2017). DOI 10.1140/epjc/s10052-017-5199-5
34. M. Tanabashi, et al., Phys. Rev. **D98**(3), 030001 (2018). DOI 10.1103/PhysRevD.98.030001
35. V. Bertone, et al., Eur. Phys. J. **C77**(12), 837 (2017). DOI 10.1140/epjc/s10052-017-5407-3
36. A. Kusina, F.I. Olness, I. Schienbein, T. Jezo, K. Kovarik, T. Stavreva, J.Y. Yu, Phys. Rev. **D88**(7), 074032 (2013). DOI 10.1103/PhysRevD.88.074032
37. H. Paukkunen, P. Zurita, JHEP **12**, 100 (2014). DOI 10.1007/JHEP12(2014)100
38. A. Buckley, J. Ferrando, S. Lloyd, K. Nordström, B. Page, M. Rüfenacht, M. Schönherr, G. Watt, Eur. Phys. J. C **75**, 132 (2015). DOI 10.1140/epjc/s10052-015-3318-8
39. S. Alekhin, et al., Eur. Phys. J. **C75**(7), 304 (2015). DOI 10.1140/epjc/s10052-015-3480-z
40. S. Chatrchyan, et al., JHEP **02**, 013 (2014). DOI 10.1007/JHEP02(2014)013
41. G. Aad, et al., JHEP **05**, 068 (2014). DOI 10.1007/JHEP05(2014)068
42. A.M. Sirunyan, et al., Submitted to: Eur. Phys. J. (2018)
43. T. Stavreva, F.I. Olness, I. Schienbein, T. Jezo, A. Kusina, K. Kovarik, J.Y. Yu, Phys. Rev. **D85**, 114014 (2012). DOI 10.1103/PhysRevD.85.114014
44. V. Bertone, et al., PoS **DIS2018**, 015 (2018). DOI 10.22323/1.316.0015
45. M.A.G. Aivazis, J.C. Collins, F.I. Olness, W.K. Tung, Phys. Rev. **D50**, 3102 (1994). DOI 10.1103/PhysRevD.50.3102
46. J.C. Collins, F. Wilczek, A. Zee, Phys. Rev. **D18**, 242 (1978). DOI 10.1103/PhysRevD.18.242
47. J.C. Collins, Phys. Rev. **D58**, 094002 (1998). DOI 10.1103/PhysRevD.58.094002
48. F. Bloch, A. Nordsieck, Phys. Rev. **52**, 54 (1937). DOI 10.1103/PhysRev.52.54
49. S.B. Libby, G.F. Sterman, Phys. Rev. **D18**, 4737 (1978). DOI 10.1103/PhysRevD.18.4737
50. S.B. Libby, G.F. Sterman, Phys. Rev. **D19**, 2468 (1979). DOI 10.1103/PhysRevD.19.2468
51. A. Chuvakin, J. Smith, W.L. van Neerven, Phys. Rev. **D61**, 096004 (2000). DOI 10.1103/PhysRevD.61.096004
52. A. Chuvakin, J. Smith, W.L. van Neerven, Phys. Rev. **D62**, 036004 (2000). DOI 10.1103/PhysRevD.62.036004
53. D. Napoletano, Istituto Nazionale di Fisica Nucleare | Sezione di Milano (2014)
54. I. Bierenbaum, J. Blumlein, S. Klein, Phys. Lett. **B672**, 401 (2009). DOI 10.1016/j.physletb.2009.01.057
55. F. Cascioli, P. Maierhöfer, N. Moretti, S. Pozzorini, F. Siegert, Phys. Lett. **B734**, 210 (2014). DOI 10.1016/j.physletb.2014.05.040